CASSINI RADAR'S FIRST LOOK AT TITAN. C. Elachi[1,2], S. D. Wall[2], M. D. Allison[3],Y. Anderson[2], R. Boehmer[2], P. Callahan[2], P. Encrenaz[4], E. Flamini[5], G. Francescetti[6], Y. Gim[2], G. Hamilton[2], S. Hensley[2], M. A. Janssen[2], W. T. K. Johnson[2], K. Kelleher[2], R. L. Kirk[7], R. M. Lopes[2], R. D. Lorenz[8], J. I. Lunine[8], D. O. Muhleman[9], S. J. Ostro[2], F. Paganelli[2], G. Picardi[10], F. Posa[11], L. E. Roth[2], R. Seu[10], S. Shaffer[2], L. A. Soderblom[7], B. Stiles[2], E. Stofan[12], S. Vetrella[6], R. West[2], C. A. Wood[13], L. Wye[14], and H. A. Zebker[14], [1] RADAR Team Leader, [2] Jet Propulsion Laboratory, California Institute of Technology, Pasadena, CA 91109. U.S.A., [3] Goddard Institute for Space Studies, National Aeronautics and Space Administration New York, NY 10025, U.S.A., [4] Observatoire de Paris, 92195 Meudon, France, [5] Agenzia Spaziale Italiana, 00131 Rome, Italy, [6] Facoltá di Ingegneria, 80125 Naples, Italy, [7] U. S. Geological Survey, Flagstaff, AZ 86001, U.S.A. (rkirk@usgs.gov), [8] Lunar and Planetary Laboratory, University of Arizona, Tucson, AZ 85721, U.S.A., [9] Division of Geological and Planetary Sciences, California Institute of Technology, Pasadena, CA 91125, U.S.A., [10] Universitá La Sapienza, 00184 Rome, Italy, [11] INFM and Dip. Interateneo di Fisica, Politecnico di Bari, 70126 Bari, Italy, [12] Proxemy Research, Bowie, MD 20715, U.S.A., [13] Planetary Science Institute, Tucson, AZ 85719, U.S.A., [14] Stanford University, Stanford, CA 94305, U.S.A.

Introduction: The Cassini Titan RADAR Mapper [1] is a K_u-band (13.78 GHz,λ= 2.17 cm) linear polarized RADAR instrument capable of operating in synthetic aperture (SAR), scatterometer, altimeter and radiometer modes. Radar observations on Titan passes Ta and T3 included rastered scatterometry, SAR, altimetry and rastered radiometry images of a full hemisphere in orthogonal linear polarizations. At this writing only the Ta data have been acquired, but data from both passes will be discussed in the presentation.

Radiometry: Disk-averaged brightnesses from low-resolution images are 85 K with an absolute uncertainty of 5 K, correspond to an overall surface emissivity in the neighborhood of 0.9 and are consistent with an effective average surface dielectric constant of 2 to 3. The images also show brightness temperature structure at all resolutions caused by emissivity variations (Figure 1a), with several distinct features of up to 500 km extent. The cold areas may be fractured ice producing volume scattering at K_u band, while the high-emissivity areas may be due to a low net dielectric constant surface, which could be composed of a low dielectric material like organic sludge (2.0 – 2.4) or a porous material of higher dielectric constant such as water or ammonia ice. Brightness temperature is negatively correlated with near-IR reflectivity [2]. There is also a strong negative correlation between brightness temperature and backscatter cross-section in our SAR and scatterometry data. The correlation is consistent with radiometric cold areas being caused by volume scattering within a structurally and/or compositionally heterogeneous low-loss ice.

Scatterometry: Plots of the angular dependence of scatterometry backscatter cross-section vs. incidence angle show both specular and diffuse-scattering echoes with brightnesses comparable to, or perhaps even larger than, Earth-based radar observations [3]. The presence of a specular component is unique among radar observations of icy moons of the outer planets. Since a specular term can arise only for extended, very flat (<0.5 cm at our wavelength) surfaces, it is quite likely that sections of smooth terrain—indeterminately solid or liquid—exist on the surface. At the same time, significant diffuse scatter implies that volume scattering is also an important effect. This implies that the surface must contain a layer of material quite transparent at K_u band. Normalized to a model scattering law fitted to uniform dark plains in the SAR image, the scatterometry data display substantial spatial variations that are positively correlated with near-IR reflectivity (Figure 1b).

Topography: Altimetric data have been obtained for only a small fraction of the surface so far (0.016% in Ta), and imagery of the altimetry tracks is unavailable at this writing, but the results indicate a rather smooth surface with local and perhaps regional relief of only a few hundred meters (Figure 2). The SAR data, which do not overlap the current altimetry data, potentially provide additional information about topographic relief at much higher spatial resolution and with a direct connection to specific geologic features. A simple one-dimensional approach to radarclinometry (radar shape-from-shading; [4]) provides slope and height estimates for the small subset of SAR features for which topographic shading appears more significant than intrinsic backscatter variations. These height estimates are also on the order of a few hundred meters.

SAR: Broad units have been identified in the SAR imagery (Figure 3) based on the brightness variation of backscatter and general planform shape [5]. The causes of the observed variations in backscatter observed are not completely understood at this time, but volume scattering is likely taking place. Ta data show few candidate impact craters [6], implying progressive burial of surface features or resurfacing within the relatively recent (<1 Gyr) geologic past. Other features seen in SAR imagery include flows and possible cryovolcanic calderas [7]. Radar-bright sinuous channels, associated fan-like features and flows [8] suggest the presence of transported material with different radar properties. Regions of extremely low backscatter may consist of organic material (solid or liquid) confined to local topographic minima [9]. The overall picture is of a young, geologically active surface, possibly modified as well by deposition of atmospheric chemical products.

References: [1] Elachi C. et al. (1991) *Proc IEEE, 79*, 867; Elachi C. et al. (2004) *Space Sci. Rev.*, in press. [2] Smith P. et al. (1996)

Icarus, 119, 336. [3] Campbell D. et al. (2003) *Science, 302*, 241. [4] Kirk R. L. et al. (2005) this conference. [5] Stofan E. et al. (2005) this conference. [6] Wood C. et al. (2005) this conference. [7] Lopes R. et al. (2005) this conference. [8] Paganelli C. et al. (2005) this conference. [9] Lorenz R. D. et al. (2005) this conference.

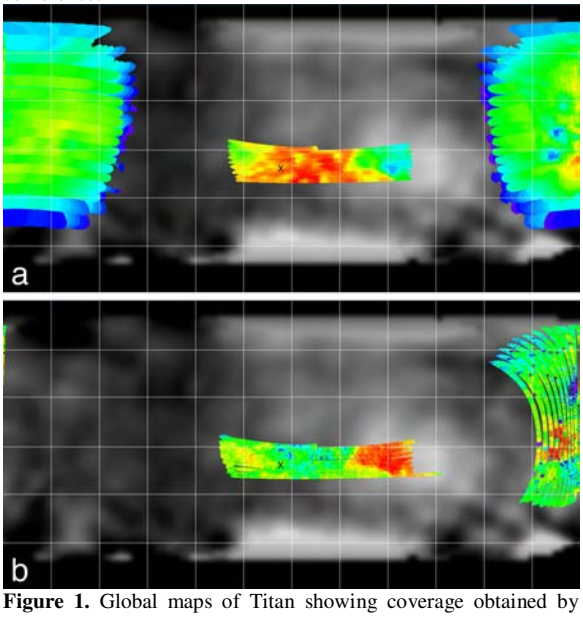

Figure 1. Global maps of Titan showing coverage obtained by rastered observation sequences during Ta flyby. Simple cylindrical projection, centered at 180° W, with 30° graticule and base map of 940 nm albedo from HST data [2]. Crosses indicate predicted location of Huygens landing point. (a) Brightness temperature corrected by Fresnel emissivity for a constant dielectric constant, from 73 K (violet) to 93 K (red). Data from multiple scans are shown with highest resolution on top. to emphasize inverse correlation with near-IR reflectivity. (b) Backscatter cross-section from scatterometry, corrected to constant incidence angle and logarithmically scaled.

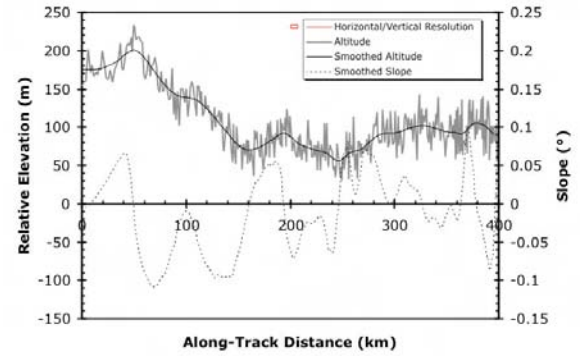

Figure 2. Ta altimetry profile. Raw elevations relative to a 2575-km sphere (gray) have been smoothed (solid black line) by convolution with a Gaussian function with standard deviation 7 points (~7 km). Bidirectional slopes (dotted line) are computed from smoothed elevations. Horizontal resolution is limited to ~25 km and vertical precision of smoothed curve to ~4 m, as shown by small rectangle.

Figure 3 (at right). SAR data taken by Cassini during Titan pass Ta, corrected to constant incidence angle and logarithmically scaled. Oblique cylindrical projection based on spacecraft ground track, with north approximately at right and 10° longitude x 5° latitude graticule. Area covered is 9.4 x 10^5 km^2, or 1.1% of Titan.